Full-Wave Design of Spurious Free D.R. TE Mode Band Pass Filters

Amr Abdelmonem, Ji-Fuh Liang, Hui-Wen Yao, and Kawthar A. Zaki

Abstract—**Analytic full-wave analysis and design of direct-coupled dielectric loaded bandpass filters in rectangular waveguide configuration using the TE_{10} mode with a spurious-free response up to twice the operating frequency is described. The filter has no tuning screws and is small in size. Theoretical design of the filter is supported by the experimental results. Superiority of the filter over the inductive window-coupled filter is presented. Practical issues faced while building the filter are discussed. An alternative folded configuration of the filter that allows the implementation of both the canonical elliptic function as well as the Chebychev response is also presented.**

I. Introduction

MICROWAVE filters are building blocks in multiplexer systems [1], used to separate the input signal into channels with different frequency bands. In addition to the in band requirements on the filters in terms of insertion loss and return loss, there is always an out of band requirements for having a spurious-free response. The motivation behind this work is to develop miniature band pass filters with a spurious-free response up to twice the operating filter frequency, that can be used in multiplexer applications.

Conventional band pass filters using dielectric resonators [2] or evanescent mode coupling [3] have a poor stopband performance in the form of higher order resonances. A simple way of eliminating these spurious transmissions is by using a low-pass filter at the output, but this will increase the insertion loss. A recent design [4] in a cylindrical air-filled waveguide configuration uses a TM mode which results in a wide, spurious-free stop band, but this configuration suffers from lower Q. Another approach is to use a slightly deformed cylindrical dielectric resonator [5] in order to control the higher order modes. Finally the use of evanescent mode band-pass irises tuned to the dielectric resonators center frequency [6] can suppress the spurious modes.

In this paper a new type of miniature dielectric band pass filter [7] is analyzed showing its superiority over other types in their stop band performance. Two configurations of the filter are presented in Section II, and their performance is compared to the inductive-window filter showing the new configuration's superior stop-band performance. One of the new configurations allows the implementation of both the canonical elliptic as well as the Chebychev response. An analytical full-wave analysis and design procedure is given. In Section III some of the practical issues in the implementation of the block filter are discussed, and the measured responses of an experimental filter are presented. Conclusions and discussions are in Section IV.

Manuscript received April 4, 1994; revised June 27, 1994.

The authors are with the Department of Electrical Engineering, University of Maryland, College Park, MD 20742 USA.

IEEE Log Number 9408557.

II. Filter Design and Comparison to an Inductive Window Filter

A. Block Filter

The filter analyzed consists of resonator blocks of high dielectric constant ϵ_{r1} separated by blocks of a low dielectric constant material (ϵ_{r2}) which serve as coupling sections. Both types of blocks have the same cross section as shown in Fig. 1(a). Fig. 1(b) shows the inductive window filter [8] where coupling is achieved by the smaller cross section windows. This structure has a homogeneous dielectric material of ϵ_{r1} for both resonator and coupling section. The full-wave field analysis of the direct coupled filter of Fig. 1(a) is simple. An incident TE_{10} mode will not excite any higher order modes as it propagates from one region to the other since both regions have the same cross section. Following the standard synthesis procedure [9] for coupled resonators filters and starting from the lumped-element prototype, the values of building block impedance inverters separated by half guide wave line lengths are obtained [9]. The inverters are related to the S-parameters of a coupling section as shown in Fig. 2. The S-parameters for the TE_{10} mode of the coupling section consisting of a cut off waveguide of length ℓ at reference planes A-A and B-B in the propagating waveguides filled with dielectric (ϵ_{r1}) shown in Fig. 2(a) are given by

$$S_{11} = S_{22} = \frac{\frac{j}{2}\left(\frac{\beta}{\alpha} + \frac{\alpha}{\beta}\right)\sinh(\alpha l)}{\cosh(\alpha l) + \frac{j}{2}\left(\frac{\beta}{\alpha} - \frac{\alpha}{\beta}\right)\sinh(\alpha l)} \tag{1}$$

$$S_{12} = S_{21} = \frac{1}{\cosh(\alpha l) + \frac{j}{2}\left(\frac{\beta}{\alpha} - \frac{\alpha}{\beta}\right)\sinh(\alpha l)} \tag{2}$$

where

$$\alpha^2 = \left(\frac{\pi}{a}\right)^2 - \epsilon_{r2}k_0^2, \quad \beta^2 = \epsilon_{r1}k_0^2 - \left(\frac{\pi}{a}\right)^2,$$
$$k_0 = \frac{2\pi}{\lambda_0}, \quad \lambda_0 = \frac{c}{f_0}$$

a is the waveguide width and f_0 is the frequency.

From (1) and the relationships in Fig. 2, the length of the coupling section l required to realize an impedance inverter K can be shown to be given by

$$l = \frac{1}{\alpha}\tanh^{-1}\frac{1 - K^2}{\sqrt{1 + K^2\{(\frac{\beta}{\alpha})^2 + (\frac{\alpha}{\beta})^2\} + K^4}}. \tag{3}$$

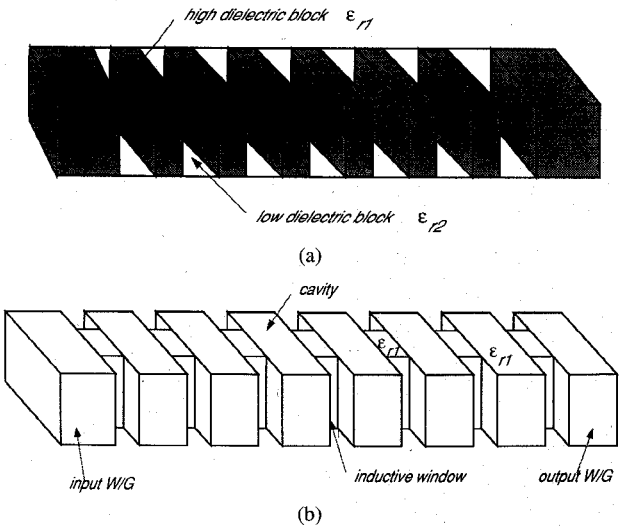

Fig. 1. (a) Six-pole direct-coupled filter. (b) Six-pole inductive window-coupled filter.

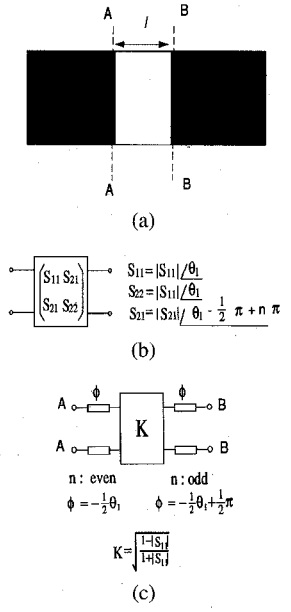

Fig. 2. (a) Coupling evanescent waveguide section. (b) Scattering matrix of a lossless, symmetrical reciprocal junction (coupling section). (c) A circuit representation of (b).

The ith resonator length L_i (i.e., the dielectric filled waveguide sections) is half a guide wavelength in the dielectric reduced by $(\phi_{i-1}+\phi_i)$ where the values of the phases ϕ_{i-1} and ϕ_i are obtained from the previous and next inverters respectively. The length of the dielectric resonator L_i sandwiched between the two inverters $K_{i-1,i}$ and $K_{i,i+1}$ can also be given to be

$$\beta L_i = \pi - \frac{1}{2}(\theta_{i-1}+\theta_i) \tag{4}$$

where

$$\theta_i = \frac{\pi}{2} - \tan^{-1}\frac{(1-K_{i,i+1}^2)(\frac{\beta}{\alpha}-\frac{\alpha}{\beta})}{\sqrt{1+K_{i,i+1}^2\{(\frac{\beta}{\alpha})^2+(\frac{\alpha}{\beta})^2\}+K_{i,i+1}^4}}. \tag{5}$$

Consequently, if the ϕ's are large, the resonator lengths decrease and the higher-order longitudinal resonant mode will have a higher resonant frequency, thus widening the filters spurious-free stop bands.

TABLE I

l_1 cavity	0.077	0.072	0.072	0.072'	0.072	0.077	
l_2 coupling	0.122	0.292	0.343	0.351	0.343	0.292	0.122

TABLE II

l_1 cavity	0.152	0.181	0.181	0.181	0181	0.152	
l_2 coupling	0.071	0.067	0.095	0.099	0.095	0.067	0.071

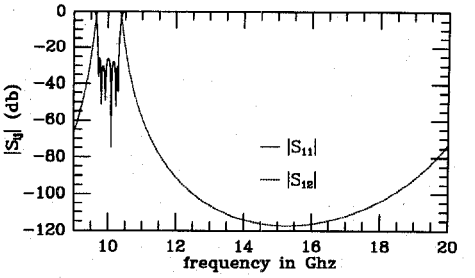

Fig. 3. Computed frequency response of a six-pole Chebychev direct coupled band pass filter with $a = 0.34''$, $b = 0.14''$, $\epsilon_{r1} = 9.6$, and $\epsilon_{r2} = 1.0$.

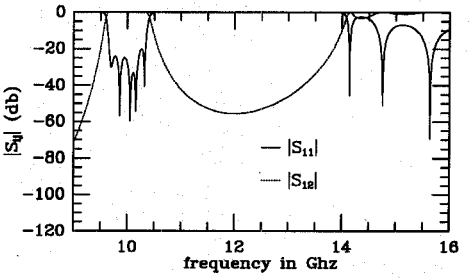

Fig. 4. Computed frequency response of a six-pole Chebychev inductive window band pass filter with $a = 0.34''$, $b = 0.14''$, and $\epsilon_{r1} = 9.6$.

Tables I and II show the dimensions of two six-pole filters: the new and the inductive window filter respectively. It is clear that the lengths of the resonator sections in the first is smaller than those of the second which results in pushing the higher order longitudinal mode to almost twice the operating frequency.

The response of a six-pole Chebychev filter with center frequency 10 GHz and bandwidth of 800 MHz is shown in Fig. 3 using dielectric blocks of $\epsilon_{r1} = 9.6$ and $\epsilon_{r2} = 1.0$. The spurious resonance comes from the higher order longitudinal mode which is the TE_{102} mode. The response of a similar inductive windows filter is shown in Fig. 4.

B. The Canonical Elliptic Filter Configuration

It is known that the elliptic function filter response is superior to the Chebychev response because of the finite transmission zeros in the stop band. Thus the elliptic function filter meets a given set of specifications by using fewer electrical cavities [9]. The elliptic function response has been realized by dual-mode circular and square waveguides [10]. The canonical form of the elliptic function filter has also been realized using single-mode TE_{101} waveguide cavities [12]. The

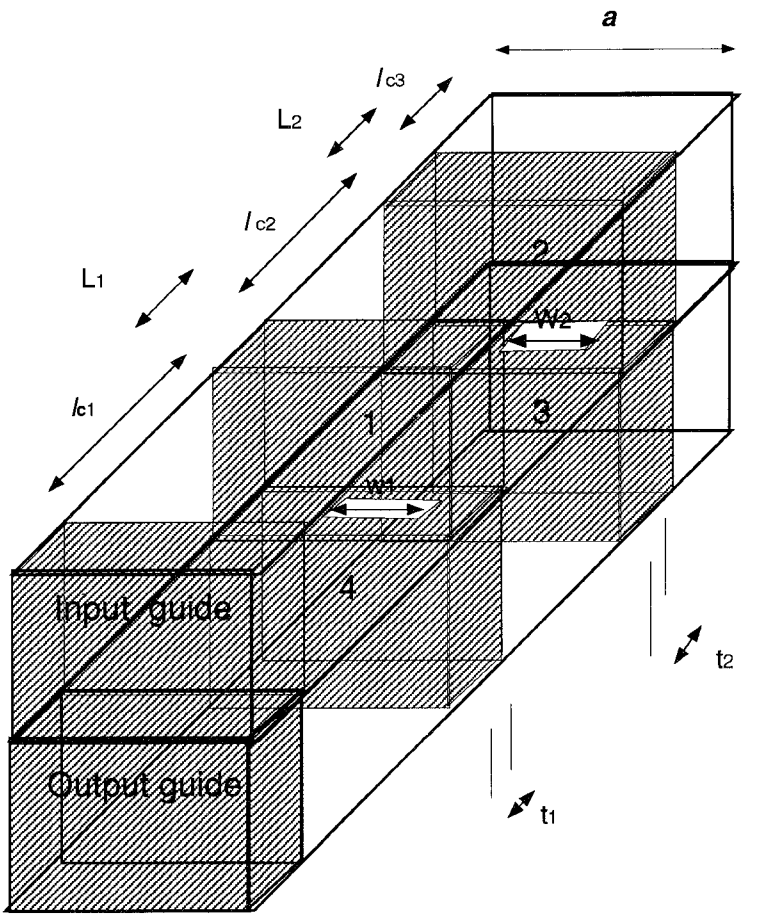

Fig. 5. A four-pole elliptic function filter.

same configuration can be realized using dielectric loading as shown in Fig. 5, which shows an example of a four-pole filter. The filter consists of two identical halves, each half consists of direct-coupled set of dielectric resonator blocks separated by evanescent waveguide sections. Each resonator of one half is coupled to the corresponding resonator in the other half through a slot in the common boundary between the two halves. In this case controlling the position of the slots can provide either electric or magnetic coupling which are of opposite sign. If the coupling hole is placed at the center of the block as in the case between cavities 1 and 4 electric coupling is achieved, while placing the hole at the end of the block provides magnetic coupling.

The analysis of this structure is more complicated than the simple block filter presented in Section II-A. The presence of the coupling holes in the common wall introduces discontinuities and higher order mode interaction. A full-wave analysis is needed in order to accurately analyze or design the filter. Consider the cross sectional view of part of the filter containing only cavities 2 and 3 shown in Fig. 6(a). The structure is a two-port structure with the input at plane A–A and the output at plane B–B. Due to the symmetry at the middle, the modal two-port S-parameters can be obtained using even and odd mode excitation (with perfect electric wall (PEW) or perfect magnetic wall (PMW) at the middle) as shown in Fig. 6(b). Only one half of the structure needs to be analyzed. The modal S-parameters of the two-port are given in terms of the even and odd one-port modal S-parameters of half the structure by

$$S_{11} = S_{22} = \frac{1}{2}(S_{11E} + S_{11O}) \tag{6}$$

$$S_{12} = S_{21} = \frac{1}{2}(S_{11E} - S_{11O}) \tag{7}$$

where S_{11E} and S_{11O} are the even and odd modal one port S-parameters of half the structure, respectively.

The problem is then reduced to solving the one port modal S-parameters of the structure shown in Fig. 7(a) for both cases (PEW and PMW). The cross section at A is a rectangular guide, at B is an inhomogeneous T shaped structure and at C is just another rectangular guide of different dielectric constant. The problem can be solved by applying the method of mode matching twice and cascading the generalized scattering matrices. First the mode matching method is used to find modes in the T-shaped structure. The modes in this case are hybrid modes and details of the solution are given in the Appendix. A second mode matching is again used to solve the junction discontinuity between rectangular waveguide and T-shaped structure (TSS) in order to obtain the modal S-parameters. The transverse fields in each region can be expressed in terms of incident and reflected waves:

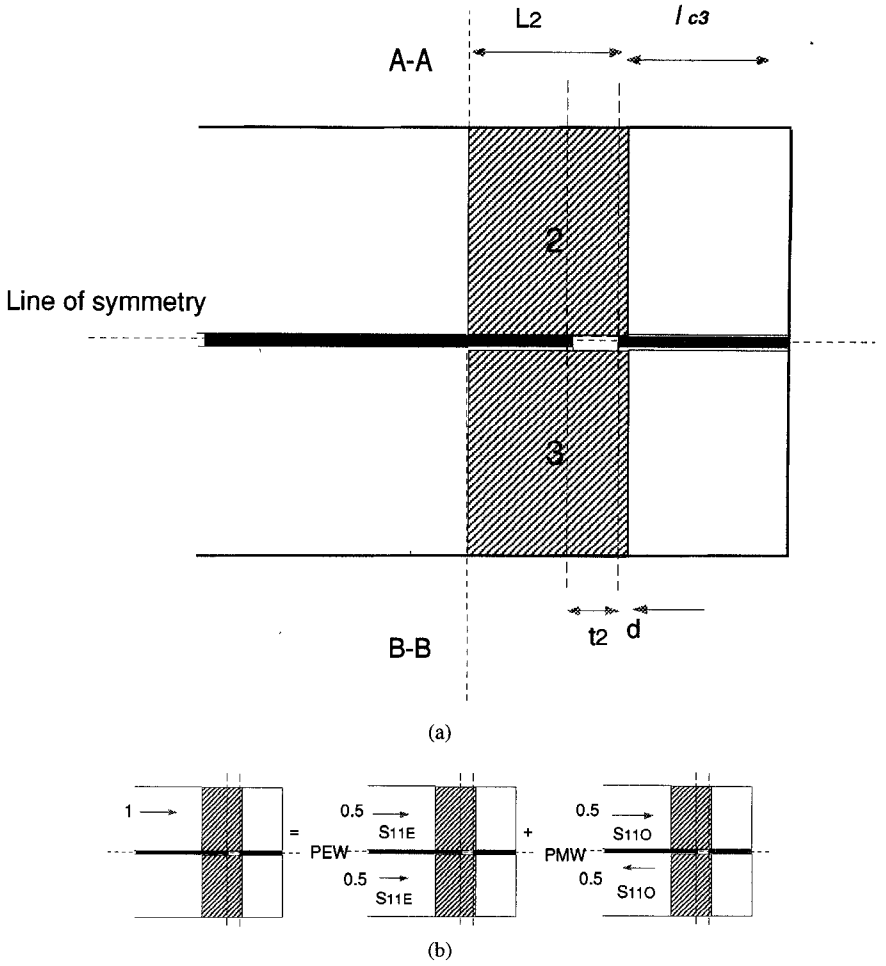

Fig. 6. (a) Cross-sectional view of the filter showing only cavities 2 and 3. (b) Illustration of the even and odd mode excitation with the use of perfect electric wall and perfect magnetic wall.

For region A,

$$\bar{E}_{tA} = \sum_{i=1}^{N} \left[A_i^+ e^{-\gamma_{Ai} z} + A_i^- e^{\gamma_{Ai} z}\right] \hat{e}_{Ai} \tag{8}$$

$$\bar{H}_{tA} = \sum_{i=1}^{N} \left[A_i^+ e^{-\gamma_{Ai} z} - A_i^- e^{\gamma_{Ai} z}\right] \hat{h}_{Ai} \tag{9}$$

where $\hat{e}_{Ai}$ and $\hat{h}_{Ai}$ are the normal modes transverse electric and magnetic fields, respectively; γ_{Ai} is the propagation constant of each mode; and N is the number of modes, including both TE & TM modes. Coefficients A_i^+ are the incident waves from $z > 0$ on the junction, and A_i^- are the reflected waves from the junction.

Similarly, for region B,

$$\bar{E}_{tB} = \sum_{j=1}^{M} \left[B_j^+ e^{-\gamma_{Bj} z} + B_j^- e^{\gamma_{Bj} z}\right] \hat{e}_{Bj} \tag{10}$$

$$\bar{H}_{tB} = \sum_{j=1}^{M} \left[B_j^+ e^{-\gamma_{Bj} z} - B_j^- e^{\gamma_{Bj} z}\right] \hat{h}_{Bj} \tag{11}$$

where M is the number of the hybrid modes, and B_j^+ and B_j^- are the incident and reflected waves, respectively. The relationships giving A_i^-, B_i^- in terms of B_j^+, and A_j^+ can be described by a two-port modal scattering network. Matching the tangential fields, and using the orthogonality relations of modes in each region, these two-port modal S-parameters can be found to be

$$\begin{bmatrix} A^- \\ B^+ \end{bmatrix} = \begin{bmatrix} S_{11} & S_{12} \\ S_{21} & S_{22} \end{bmatrix} \begin{bmatrix} A^+ \\ B^- \end{bmatrix} \tag{12}$$

where the submatrices S_{11}, S_{12}, S_{21}, and S_{22} have the orders $N \times N$, $N \times M$, $M \times N$and $M \times M$, respectively.

The corresponding modal scattering parameter network is given in Fig. 7(b), where the two modal scattering parameter networks S^{I} and S^{II} represent the two junction discontinuities between TSS and rectangular waveguide. The modal scattering parameter S^{III} represent the discontinuity from guide A to C. By cascading the two networks with the four waveguide lengths of cross sections A, B, A and C as shown in Fig. 7(b) and introducing a short at the output the one-port modal S-parameters are obtained. (This has to be computed twice for PEW and PMW in cross section B). Fig. 8(a) shows the effect of width t_2 on magnetic coupling when the coupling slot is at the end of the block ($d = 0$ in Fig. 7(a)), by increasing the width t_2 the coupling increases. Fig. 8(b) shows how the coupling changes sign when the

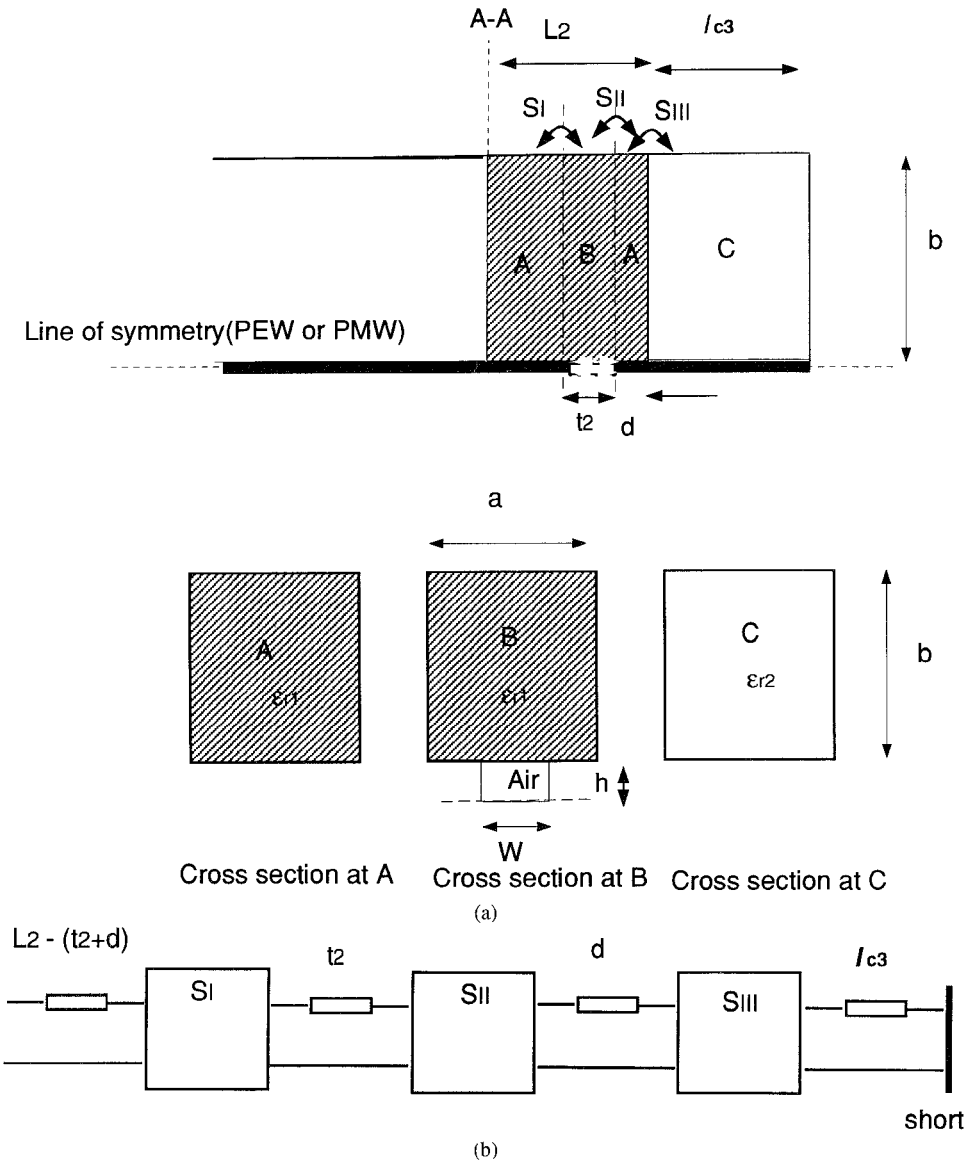

Fig. 7. (a) The structure analyzed. (b) Equivalent scattering parameter network.

slot is at the middle of the block ($d = \frac{(L_2 - t_2)}{2}$) versus the width t_2. In this case the coupling is electric (negative) for small values of t_2 where electric field is maximum and the magnetic field is minimum then the coupling starts to increase (becomes less negative) due to the magnetic field contribution and then ends up being magnetic (positive) coupling.

Following the same procedure as in the Chebychev filter, the values of the building-block impedance inverters are obtained. The lengths of the coupling sections l_{c1} and l_{c2} (see Fig. 5) are found from (3). From the calculated S-parameters between planes A-A and B-B shown in Fig. 6(a), the thickness t_2 can be adjusted to give the required coupling K_{23}. Correction for the resonator lengths as discussed before is needed for resonators 2 and 3 ((4) and (5)). Similarly the width t_1 is determined, and correction of the resonator lengths 1 and 4 are obtained. The in-band and the out-band performance of a four-pole elliptic filter is shown in Fig. 9(a) and (b), respectively.

III. Experimental Results

A six-pole Chebychev direct-coupled filter with a center frequency of 10 GHz and bandwidth of 800 MHz was designed with dimensions as shown in Table I. The first filter built had an upward shift of 400 MHz in its center frequency which was attributed to that the effective dielectric constant was not 9.6 as used in the design, but 9.08. Subsequently the effect of the presence of a small air gap between the dielectric block and the metallic enclosure on the propagation constant as shown in Fig. 10(a) was investigated. An effective dielectric constant of the block is defined as if there was no air gap and the cross section is totally filled by a material of dielectric constant ϵ_{reff}. From calculated β of the structure shown in Fig. 10(a) the effective dielectric constant is computed. In Fig. 10(b) the effective dielectric constant is plotted versus the air gap. The air gap in the a dimension has no effect since the gap transverse electric field is almost zero. The gap in the b dimension, however, has a significant effect on the propagation constant. Since the first

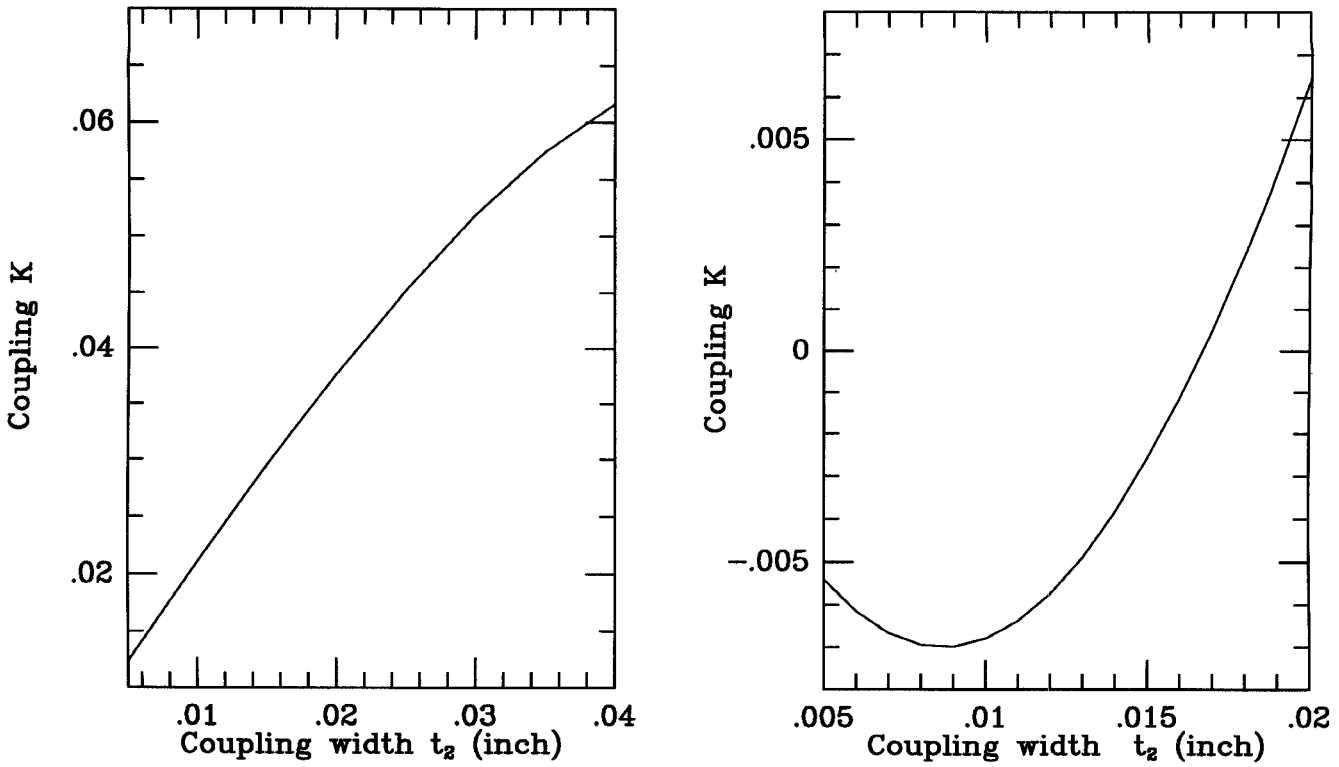

Fig. 8. (a) The effect of width t_2 on magnetic coupling, ($a = 0.34''$, $b = 0.14''$, $f = 10.0$ GHz, $\epsilon_{r1} = 9.6$, $w = 0.2''$, $h = 0.015''$, and $l_{c3} = 0.25''$). (b) The effect of width t_2 on coupling, ($a = 0.34''$, $b = 0.14''$, $f = 10.0$ GHz, $\epsilon_{r1} = 9.6$, $w = 0.06''$, $h = 0.015''$, and $l_{c3} = 0.25''$).

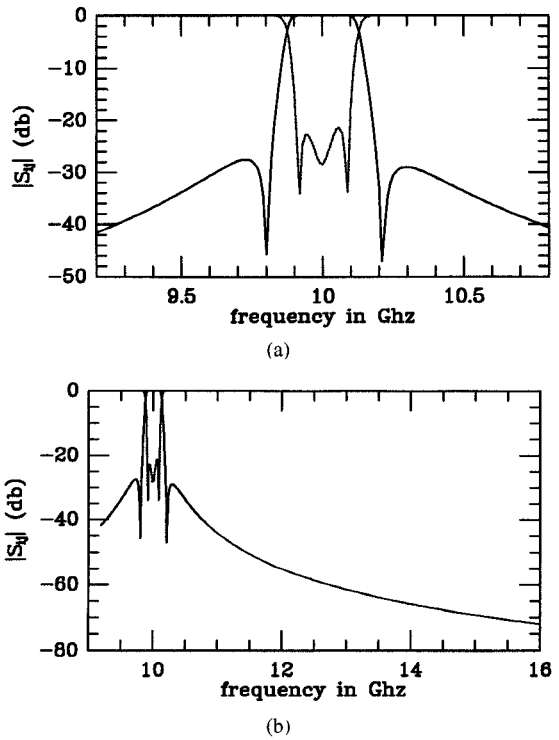

Fig. 9. Computed response of the filter. (a) The in band response. (b) The out band performance. ($l_{c1} = 0.209, l_{c2} = 0.4748, l_{c3} = 0.25$, $L_1 = 0.07522$, $L_2 = 0.0740$, $t_1 = 0.019, t_2 = 0.01$, $w_1 = 0.2$, $w_2 = 0.06$, $a = 0.34''$, $b = 0.14''$, and $\epsilon_{r1} = 9.6$).

filter built had an air gap about 0.001 $''$ in the b dimension the effective dielectric constant was 9.08 which explains the shift in the filter frequency. The interior of the filter's Aluminum enclosure was overplated by silver. The filter was assembled again with no air gaps by heating the enclosure to expand and then inserting the dielectric blocks inside the metallic housing. Fig. 11 shows a photograph of the partially assembled filter. The measured response of the filter is shown in Fig. 12(a) and (b). Coupling to the input and output is realized by coaxial probes instead of the infinite waveguide assumed in the model. This caused the return loss to be degraded to about 10 dB. The filter insertion loss is about 0.4 dB and the connector loss is 0.2 dB.

IV. Conclusion

A new type of miniature dielectric loaded band pass filter is built with a wide spurious free stop band. Superiority over other types of filters is explained. The filter, in addition to being small in size and low loss, does not need any tuning. Experimental work shows the importance of avoiding air gaps between the dielectric and the enclosure. The folded configuration of the block filter allows the implementation of both the canonical elliptic function as well as the Chebychev filter. Rigorous full wave analysis of the cross coupling structure is presented and used in the elliptic function filter design.

Appendix
Modes in the T-Shaped Structure

The T-shaped structure is divided into two regions I and II as shown in Fig. A-1. For the case of electric wall at the line of symmetry. The structure is divided into two regions, and

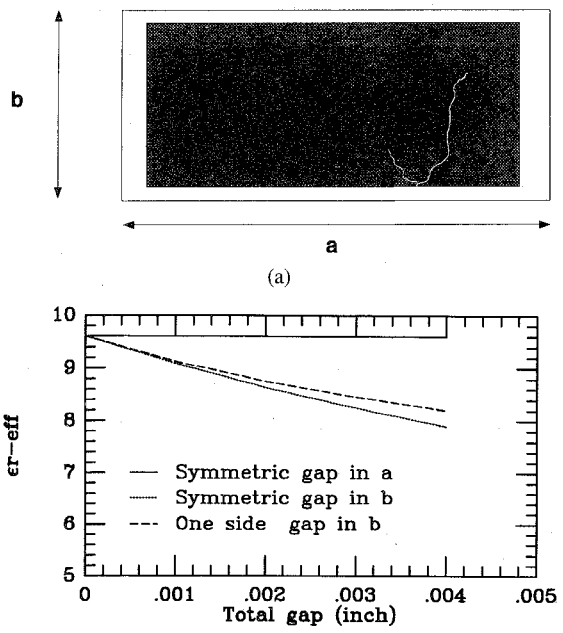

Fig. 10. (a) Partially filled dielectric loaded waveguide with a gap in both a and b dimensions. (b) Effective dielectric constant with a partially dielectric loaded rectangular waveguide with $a = 0.34''$, $b = 0.14''$, $f = 10.0$ GHz, and $\epsilon_{r1} = 9.6$.

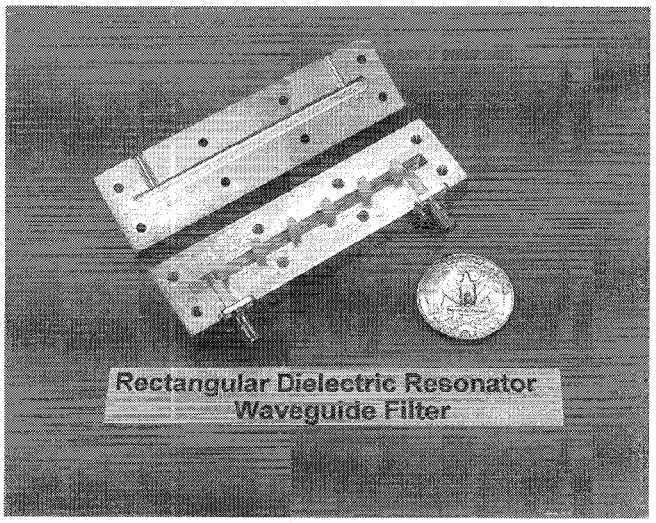

Fig. 11. Photograph of the filter.

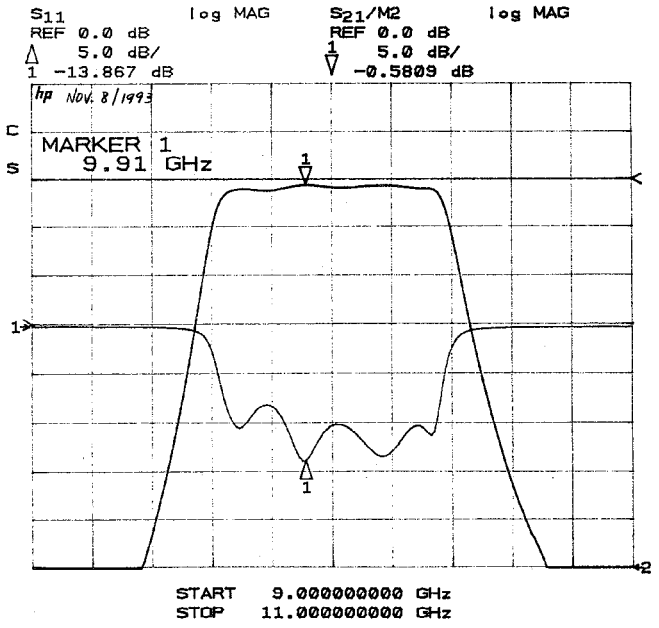

Fig. 12. (a) Measured filter response. (b) Measured filter response showing out of band performance.

the field in each region is expanded in terms of orthogonal functions as follows:

For region I,

$$E_{z1} = \sum_{n=1}^{N} A_{1n} k_{c1}^2 \sin(k_{x1n}x)\sin(k_{y1n}(b-y)) \quad \text{(A1)}$$

$$\frac{j\omega\mu}{\gamma} H_{z1} = \sum_{n=0}^{N} B_{1n} k_{c1}^2 \cos(k_{x1n}x)\cos(k_{y1n}(b-y)) \quad \text{(A2)}$$

$$E_{x1} = -\gamma \sum_{n=1}^{N} A_{1n} k_{x1n} \cos(k_{x1n}x)\sin(k_{y1n}(b-y)) - \gamma \sum_{n=0}^{N} B_{1n} k_{y1n} \cos(k_{x1n}x)\sin(k_{y1n}(b-y)) \quad \text{(A3)}$$

$$E_{y1} = \gamma \sum_{n=1}^{N} A_{1n} k_{y1n} \sin(k_{x1n}x)\cos(k_{y1n}(b-y)) - \gamma \sum_{n=0}^{N} B_{1n} k_{x1n} \sin(k_{x1n}x)\cos(k_{y1n}(b-y)) \quad \text{(A4)}$$

$$H_{x1} = -j\omega\epsilon_1 \sum_{n=1}^{N} A_{1n} k_{y1n} \sin(k_{x1n}x)\cos(k_{y1n}(b-y)) + \frac{\gamma^2}{j\omega\mu} \sum_{n=0}^{N} B_{1n} k_{x1n} \sin(k_{x1n}x)\cos(k_{y1n}(b-y)) \quad \text{(A5)}$$

$$H_{y1} = -j\omega\epsilon_1 \sum_{n=1}^{N} A_{1n} k_{x1n} \cos(k_{x1n}x)\sin(k_{y1n}(b-y)) - \frac{\gamma^2}{j\omega\mu}\sum_{n=0}^{N} B_{1n}k_{y1n}\cos(k_{x1n}x)\sin(k_{y1n}(b-y)) \tag{A6}$$

where

$$k_{x1n}^2 + k_{y1n}^2 = \gamma^2 + k_1^2 = k_{c1}^2,$$
$$k_{x1n} = \frac{n\pi}{a} \quad \text{and} \quad k_1^2 = \omega^2\mu\epsilon_1 \tag{A7}$$

γ and k_{c1}, are the propagation constant and the cut-off wave number in region I.

For region II,

$$E_{z2} = \sum_{m=1}^{M} A_{2m}k_{c2}^2 \sin(k_{x2m}(x-a_1))\sin(k_{y2m}(h+y)) \tag{A8}$$

$$\frac{j\omega\mu}{\gamma}H_{z2} = \sum_{m=0}^{M} B_{2m}k_{c2}^2\cos(k_{x2m}(x-a_1)) \times \cos(k_{y2m}(h+y)) \tag{A9}$$

$$E_{x2} = -\gamma\sum_{m=1}^{M} A_{2m}k_{x2m}\cos(k_{x2m}(x-a_1)) \times \sin(k_{y2m}(h+y)) + \gamma\sum_{m=0}^{M} B_{2m}k_{y2m} \times \cos(k_{x2m}(x-a_1)\sin(k_{y2m}(h+y)) \tag{A10}$$

$$E_{y2} = -\gamma\sum_{m=1}^{M} A_{2m}k_{y2m}\sin(k_{x2m}(x-a_1)) \times \cos(k_{y2m}(h+y)) - \gamma\sum_{m=0}^{M} B_{2m}k_{x2m}\sin(k_{x2m}(x-a_1)) \times \cos(k_{y2m}(h+y)) \tag{A11}$$

$$H_{x2} = j\omega\epsilon_2\sum_{m=1}^{M} A_{2m}k_{y2m}\sin(k_{x2m}(x-a_1)) \times \cos(k_{y2m}(h+y)) + \frac{\gamma^2}{j\omega\mu}\sum_{m=0}^{M} B_{2m}k_{x2m}\sin(k_{x2m}(x-a_1)) \times \cos(k_{y2m}(h+y)) \tag{A12}$$

$$H_{y2} = -j\omega\epsilon_2\sum_{m=1}^{M} A_{2m}k_{x2m}\cos(k_{x2m}(x-a_1)) \times \sin(k_{y2m}(h+y)) + \frac{\gamma^2}{j\omega\mu}\sum_{m=0}^{M} B_{2m}k_{y2m}\cos(k_{x2m}(x-a_1)) \times \sin(k_{y2m}(h+y)) \tag{A13}$$

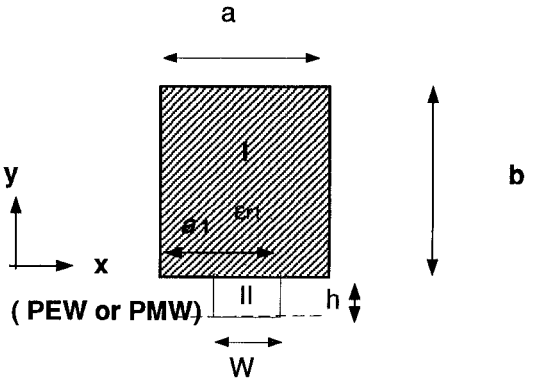

Fig. A-1. T-shaped structure cross section.

where

$$k_{x2m}^2 + k_{y2m}^2 = \gamma^2 + k_2^2 = k_{c2}^2,$$
$$k_{x2m} = \frac{m\pi}{w} \quad \text{and} \quad k_2^2 = \omega^2\mu\epsilon_2 \tag{A14}$$

γ and k_{c2}, are the propagation constant and the cut-off wave number in region I.

By applying the boundary condition at $y = 0$, taking the inner product and using the orthogonality relation on the eigenfields in each region, the following characteristic equation is obtained.

$$\begin{bmatrix} D_1M_1 - M_3 & D_4 - M_4M_2 \\ D_5 - M_5M_1 & D_2M_2 - M_6 \end{bmatrix}\begin{bmatrix} A_{2m} \\ B_{1n} \end{bmatrix} = 0 \tag{A15}$$

where the matrices are

$$M_1(i,j) = (k_{c2}^2)\quad I_s(i,j), \text{ of size } N \times M$$
$$M_2(j,i) = (k_{c1}^2)\quad I_c(j,i), \text{ of size } (M+1)\times(N+1)$$
$$M_3(i,j) = \left(\frac{-j\pi}{w}\right)\quad I_c(i,j+1), \text{ of size } (N+1)\times M$$
$$M_4(i,j) = \frac{\sqrt{k_{c2}^2 - (\frac{(j-1)\pi}{w})^2}}{k_{c2}^2}\tan\sqrt{k_{c2}^2 - \left(\frac{(j-1)\pi}{w}\right)^2}h \times I_c(i,j)\quad \frac{\delta_j}{w}, \text{ of size } (N+1)\times(M+1)$$
$$M_5(i,j) = k_1^2\frac{\sqrt{k_{c1}^2 - (\frac{j\pi}{a})^2}}{k_{c1}^2}\cot\sqrt{k_{c1}^2 - \left(\frac{j\pi}{a}\right)^2}b \times I_s(j,i)\quad \frac{2}{a}, \text{ of size } M\times N$$
$$M_6(i,j) = \gamma^2\left(\frac{(j-1)\pi}{a}\right)\quad I_s(j-1,i), \text{ of size } M\times(N+1)$$
$$D_1(j-1,j) = \left(\frac{-j\pi}{a}\right)\frac{1}{k_{c1}^2}, \text{ of size } (N+1)\times N$$
$$D_2(j,j+1) = \frac{\gamma^2}{k_{c2}^2}\left(\frac{j\pi}{w}\right), \text{ of size } M\times(M+1)$$
$$-D_4(i,j) = -\sqrt{k_{c1}^2 - \left(\frac{(j-1)\pi}{a}\right)^2}\tan\sqrt{k_{c1}^2 - \left(\frac{(j-1)\pi}{a}\right)^2}b \times I_s(i,j)\frac{a}{\delta_j}, \text{ of size } (N+1)\times(N+1)$$

$$D_5(i,j) = -k_2^2 \frac{\sqrt{k_{c2}^2 - (\frac{j\pi}{w})^2}}{k_{c2}^2} \quad \cot\sqrt{k_{c2} - \left(\frac{j\pi}{w}\right)^2}\, h \times I_c(i,j)\frac{2}{w}, \text{ of size } M \times M \tag{A16}$$

where $\delta_j = 1$ for $j = 1$ and $\delta_j = 2$ for other values of j.

$$I_c(i,j) = \int_{w+a_1}^{a_1} \cos\left(\frac{i\pi}{a}x\right)\cos\left(\frac{j\pi}{w}(x-a_1)\right)dx \tag{A17}$$

$$I_s(i,j) = \int_{w+a_1}^{a_1} \sin\left(\frac{i\pi}{a}x\right)\sin\left(\frac{j\pi}{w}(x-a_1)\right)dx. \tag{A18}$$

Solving the determinant (15), will give γ's of the structure and consequently the modes.

The same procedure can be repeated for the case of perfect magnetic wall at the line of symmetry.

REFERENCES

[1] A. E. Atia, "Computer-aided design of waveguide multiplexers," *IEEE Trans. Microwave Theory Tech.*, vol. 22, pp. 332–336, Mar. 1974.

[2] H.-C. Chang and K. Zaki, "Evanescent-mode coupling of dual-mode rectangular waveguide filters," *IEEE Trans. Microwave Theory Tech.*, vol. 39, pp. 1307–1312, Aug. 1991.

[3] Y. Kobayashi and M. Minegishi, "Precise design of a band pass filter using high-Q dielectric ring resonators," *IEEE Trans. Microwave Theory Tech.*, vol. 35, pp. 1156–1160, Dec. 1987.

[4] R. R. Bonetti and A. E. Williams, "A narrow band filter with a wide spurious-free stopband," in *IEEE 1992 Microwave Theory Tech. Symp. Dig.*, 1992, pp. 1331–1333.

[5] R. R. Mansour, "Dual-mode dielectric resonator filters with improved spurious performance," in *1993 IEEE Microwave Theory Tech. Symp. Dig.*, 1993, pp. 439–442.

[6] R. V. Snyder, "Dielectric resonator filters with wide stopbands," *IEEE Trans. Microwave Theory Tech.*, pp. 2100–2103, Nov. 1992.

[7] K. Wakino, T. Nishikawa, and Y. Ishikawa, "Miniaturization of dielectric resonator filters for mobile communications," in *Microwave Theory Tech. Workshop-Filters and multiplexers for mobile communications*, 1993.

[8] J.-F. Liang and K. Zaki, "Cad of microwave junctions by polynomial curve fitting," in *1993 IEEE Microwave Theory Tech. Symp. Dig.*, 1993, pp. 451–454.

[9] G. L. Mathaei, L. Young, and E. M. T. Jones, *Microwave filters Impedance-Matching Networks and Coupling Structures*. New York: McGraw-Hill, 1964.

[10] A. E. Atia and A. E. Williams, "New type of bandpass filters for satellite transponders," *COMSAT Tech. Rev.*, vol. 1, no. 1, pp. 21–43, Fall 1971.

[11] ——, "Narrow bandpass waveguide filters," *IEEE Trans. Microwave Theory Tech.*, vol. 20, pp. 258–265, Apr. 1972.

[12] A. E. Atia, A. E. Williams, and R. W. Newcomb, "Narrow band multiple coupled cavity synthesis," *IEEE Trans. Circuits Syst.*, vol. CAS-21, pp. 649–655, Sept. 1974.

Amr Abdelmonem, for a photograph and a biography, see p. 2380 of the December 1994 issue of this TRANSACTIONS.

Ji-Fuh Liang, for a biography, see p. 2830 of the December 1994 issue of this TRANSACTIONS.

Hui-Wen Yao, for a photograph and a biography, see p. 2379 of the December 1994 issue of this TRANSACTIONS.

Kawthar A. Zaki, for a photograph and a biography, see p. 2830 of the December 1994 issue of this TRANSACTIONS.